Mapping cortical excitability in the human dorsolateral prefrontal cortex

Juha Gogulski[1,2,*], Christopher C. Cline[1,*], Jessica M. Ross[3,1], Jade Truong[1], Manjima Sarkar[1], Sara Parmigiani[1], Corey J. Keller[1,3,δ]

[1]Department of Psychiatry & Behavioral Sciences, Stanford University Medical Center, Stanford, CA, 94305, USA

[2]Department of Clinical Neurophysiology, HUS Diagnostic Center, Clinical Neurosciences, Helsinki University Hospital and University of Helsinki, Helsinki, FI-00029 HUS, Finland

[3]Veterans Affairs Palo Alto Healthcare System, and the Sierra Pacific Mental Illness, Research, Education, and Clinical Center (MIRECC), Palo Alto, CA, 94394, USA

*Denotes equal contribution

[δ]Correspondence:
Corey Keller, MD, PhD
Stanford University
Department of Psychiatry and Behavioral Sciences
401 Quarry Road
Stanford, CA 94305-5797
Email: ckeller1@stanford.edu
Phone: +1 8025786292

Running title: Mapping local neural responses in the dlPFC

Keywords: Transcranial magnetic stimulation (TMS), electroencephalography (EEG), dorsolateral prefrontal cortex (dlPFC), TMS-evoked potentials (TEPs)

Abstract

Background: Repetitive transcranial magnetic stimulation (rTMS) to the dorsolateral prefrontal cortex (dlPFC) is an effective treatment for depression, but the neural response to rTMS remains unclear. TMS with electroencephalography (TMS-EEG) can probe these neural effects, but variation in TMS-evoked potentials (TEPs) across the dlPFC are not well characterized and often obscured by muscle artifact. Mapping TEPs and artifacts across dlPFC targets is needed to identify high fidelity subregions that can be used for rTMS treatment monitoring.

Objective: To characterize 'early TEPs' anatomically and temporally close (20-50 ms) to the TMS pulse and associated muscle artifacts (<20 ms) across the dlPFC. We hypothesized that TMS location and angle would affect these early TEPs and that TEP size would be inversely related to muscle artifact. We sought to identify an optimal TMS target / angle for the group and asked if individualization would be beneficial.

Methods: In 16 healthy participants, we applied single-pulse TMS to six targets within the dlPFC at two coil angles and measured EEG responses.

Results: Early TEPs were sensitive to stimulation location, with posterior and medial targets yielding larger early TEPs. Regions with high early TEP amplitude had less muscle artifact, and vice versa. The best group-level target yielded 102% larger TEP responses compared to other standard targets. Optimal TMS target differed across subjects, suggesting that a personalized targeting approach could boost the early TEP by additional 36%.

Conclusions: The early TEPs can be probed without significant muscle-related confounds in posterior-medial regions of the dlPFC. A personalized targeting approach may further enhance the signal quality of the early TEP.

Highlights:

- Early TEPs varied significantly across the dlPFC as a function of TMS target.
- TMS targets with less muscle artifact had significantly larger early TEPs.
- Selection of a postero-medial target increased early TEPs by 102% compared to anterior targets.
- Retrospective target and angle optimization increased early TEPs by an additional 36%.

1. Introduction

Repetitive transcranial magnetic stimulation (rTMS) to the dorsolateral prefrontal cortex (dlPFC) is a safe and effective treatment for medication-resistant depression (1). Despite widespread clinical adoption, however, the neural effects of rTMS treatment remain unknown. As changes in dlPFC excitability are thought to underlie the clinical effects of rTMS (2,3), brain-based metrics that track cortical excitability with high signal quality are paramount to improve our understanding of the neural effects of rTMS treatment and guide future treatment optimization.

Causal noninvasive measures of local cortical excitability exist but to date have not been well-characterized across different dlPFC treatment targets (4). Single pulses of TMS paired with electroencephalography (TMS-EEG) provide a noninvasive, causal readout of neural activity with millisecond resolution sufficient to capture treatment-related changes in cortical excitability (3). Moreover, TMS-evoked EEG potentials (TEPs (5)) outside of prefrontal cortex can be used to monitor sleep stages (6,7), measure the neural effects to electroconvulsive therapy (8), and differentiate neurovegetative states from coma (9). Despite these use cases, little is known about the TEPs across the dlPFC. This is in part due to the large TMS-induced muscle artifacts that have been difficult to remove and often confound TEPs (10). Furthermore, limited TEP studies exist that directly compare artifacts across the dlPFC. Studies have explored the relationship between TEP and artifact at one dlPFC target (2,11–13), and in more medial prefrontal locations (14), but to date characterization of early TEPs and artifacts across clinically relevant sub-regions of the dlPFC is lacking. Filling these gaps will enhance our understanding of which clinical rTMS targets could be monitored using TMS-EEG, and the role of target personalization to enhance TEP signal quality.

Here we sought to map the distribution of early TEPs and artifacts across the dlPFC. We focused on the early (20-50 ms) TEP in the left dlPFC as it represents the earliest noninvasively measurable neural response to TMS (14), reflects local cortical excitability (15), and avoids later responses (>100 ms) that in recent years have been accepted as largely off-target sensory responses (16–18). In 16 healthy participants, we applied single-pulse TMS to six clinically-relevant dlPFC locations and two coil orientations. For each target / angle combination, we computed both the early TEP and the TMS-evoked muscle artifact. Based on the anatomical distribution of facial muscles (19) which directly relates to the strength of evoked muscle artifact, we hypothesized that 1) posterior-medial regions would induce the largest early TEPs and smallest artifacts and 2) individual target / angle selection would yield larger early TEPs and motivate personalized targeting for future clinical applications. We observed that across dlPFC targets, both early TEPs and artifacts were sensitive to target location, with targets evoking larger artifacts generally associated with smaller early TEPs. The group-best target / angle location yielded early TEPs that were more than twice the size of other targets. The optimal target / angle combination for each individual produced larger early TEPs than the group-best combination, suggesting that personalized targeting strategies may be helpful for future use of dlPFC TEPs in clinical applications. Taken together, these findings inform our ability to causally measure cortical excitability across the dlPFC and offer an individualized path to maximizing brain responses with potential applications for treatment monitoring and biomarker-driven treatment optimization.

2. Methods

2.1. Participants

22 healthy participants (23-64 years old, mean=39.45, SD=13.00, seven females) were recruited into the study and provided written informed consent under a protocol approved by the Stanford University Institutional Review Board. All participants completed an online screening questionnaire with inclusion criteria as follows: aged 18-65, fluent in English, able to travel to study site, and fully vaccinated against COVID-19. Participants were also required to complete the *Quick Inventory of Depressive Symptomatology (16-item, QIDS)* self-report questionnaire and were excluded if they scored 11 or higher, indicating moderate or more severe depression (20). Additional criteria for exclusion included a lifetime history of psychiatric or neurological disorder, substance or alcohol abuse / dependence in the past month, recent heart attack (<3 months), pregnancy, the presence of any contraindications for rTMS (21,22), or usage of psychotropic medications. All eligible

participants were scheduled for two study visits on separate days to first obtain an MRI and then complete a TMS-EEG session. All enrolled participants completed an MRI pre-examination screening form provided by Richard M. Lucas Center for Imaging at Stanford University. Six subjects were excluded from the study: three before the experimental session, one for TMS intolerability assessed by delivering test single pulses before the experiment, one for lower back pain, and one for technical difficulties. All remaining 16 subjects (24-64 years old, mean=38.81, SD=13.39, three females) were included in the analyses.

2.2. Transcranial Magnetic Stimulation

Single-pulse TMS was delivered using a MagVenture Cool-B65 A/P figure-of-eight coil with a MagPro X100 stimulator (MagVenture, Denmark). A thin (0.5 mm) foam pad was attached to the TMS coil to minimize electrode movement and bone-conducted auditory artifact (23). The TMS coil was held and positioned automatically by a robotic arm (TMS Cobot, Axilum Robotics, France). MRI-based neuronavigation (Localite TMS Navigator, Localite, Germany) was used to align the coil to pre-planned individualized coil orientations for each stimulation target (see section 2.2.3). To estimate resting motor threshold (rMT), biphasic single pulses of TMS were delivered to the hand region of the left motor cortex with the coil held tangentially to the scalp and at 45° from midline. The optimal motor hotspot was defined as the coil position from which TMS produced the largest and most consistent visible twitch in relaxed right first dorsal interosseous muscle (FDI). rMT was determined to be the minimum intensity that elicited a visible twitch in relaxed FDI in ≥ 5 out of 10 pulses.

2.2.1 dlPFC Target Selection

For each subject, single-pulse TMS was delivered to six different targets within the left dlPFC (Table 1). The number of targets and spatial locations were chosen to balance the following: sampling of the anterior / posterior and medial / lateral planes in the middle frontal gyrus and sampling of the many of the utilized clinical dlPFC targets for depression (24), as shown in Fig. S1. While higher density sampling is ideal for full characterization, this number of targets allowed for sampling of much of the dlPFC and to test two different angles within a reasonable session duration for the participants. The MNI coordinates for these six targets are outlined in Table 1. The *t1* target is close to the commonly used 5 cm average clinical target (25). The *t2* target corresponds to the EEG F3 site of Herwig *et al*. 2003 (26), as presented by Cash *et al*. (24). The *t3*

target is located between the BA9 definition by Rajkowska *et al*. 1995 (27) and a treatment site with activity negatively correlated to anterior subgenual cingulate cortex (sgACC (25)). The *t4* target corresponds to a treatment site with activity that is most negatively correlated to the sgACC, as described by Fox *et al.* (25). The *t5* target is close to an rTMS target that produced clinical response in the study by Herbsman *et al*. 2009 (28). The *t6* target is close to the 5.5 cm average target of Weigand *at al*. 2018 (29). Euclidean distances between the stimulation sites of the current study are shown in Table S1, and the distances between the current targets and clinical targets are depicted in Fig. S2. The six targets were registered to each individual brain using a non-linear inverse transformation (see 2.3.).

Stimulation site	**x**	**y**	**z**	**BA**	**HCPex**	**Closest clinical target***
t1	-37	12	57	9	8av	5 cm average (Fox *et al*., 2012)
t2	-37	23	47	9	8av	EEG F3 site (Herwig *et al*., 2003)
t3	-38	33	36	46	46	Optimal FC Group Target #1 (Fox *et al*., 2012)
t4	-38	44	26	46	46	Optimal FC Group Target #2 (Fox *et al*., 2012)**
t5	-42	20	42	44 (/9)	NaN/8Av	Clinical responders (Herbsman *et al*., 2009)
t6	-32	26	52	8 (/9)	8Av	5.5cm average (Weigand *et al*., 2018)

Table 1 - MNI coordinates of the dlPFC stimulation targets. BA: Brodmann area (according to MRICron Brodmann atlas (https://www.nitrc.org/projects/mricron). HCPex: Brodmann areas according to HCPex atlas (30). *Locations of the clinical targets were extracted from a summary of Cash *et al*. 2021 (24). **Target t4 had the same MNI coordinates as a treatment site with activity that is most negatively correlated to the sgACC, as described by Fox *et al.* (25).

2.2.2. Experimental Design

The order of target / angle conditions was pseudorandomized within the session. 150 single-pulse TMS trials were collected for each experiment block. For a subset of conditions (all targets at 45°), two blocks of single pulse data were collected. For these conditions, the TEP amplitudes from each set of 150 single pulse blocks was averaged together. For each condition, single TMS pulses were delivered every 1.5 s, jittered +/- 25%. To maintain levels of attention, subjects were shown neutral

images on a screen and were instructed to keep eyes open during stimulation. Subjects were monitored throughout the experiment.

2.3. Stimulation target and intensity individualization

Electric fields (E-fields) induced by TMS were computationally modeled using SimNIBS (31,32) (v3.2.5). Subject-specific head models were generated from T1 and T2 MRIs using *headreco*. Deformation fields providing a non-linear spatial mapping from MNI coordinates to the brains of individual participants were generated using SPM12 (https://www.fil.ion.ucl.ac.uk/spm/). T1 MRIs were segmented and inverse deformation fields were created for each individual. MNI target coordinates were warped to individual space using the inverse deformation field (Fig. 1A). Given a target coordinate in individual brain space, 45° and 90° coil orientations were generated based on positioning the coil perpendicular to the nearest point on the scalp, with an additional offset to account for EEG electrode and coil foam thickness. Using a custom dipole model of the TMS coil, induced E-fields were then predicted for each coil orientation (Fig. 1B).

Maximal E-field magnitudes on the cortical surface were calculated (after rejecting the top 0.01% of values to remove outliers) to obtain an estimate of stimulation intensity at the cortical surface. Actual stimulation intensities (Fig. 1C) were set based on the experimentally-determined motor threshold multiplied by the ratio between maximal predicted E-field magnitude at the site of stimulation and at the motor hotspot, similar to the APEX MT approach (33). In theory, this procedure results in a consistent stimulation intensity at the brain across all stimulation targets, accounting for variation in anatomical parameters such as skull thickness across targets. If the calculated stimulation intensity exceeded 100% maximal stimulator output (MSO), intensities of all conditions were scaled down in such a way that the largest intensity would not exceed 100% MSO. Across all stimulation targets and subjects, the TMS intensity varied from 45 to 100% MSO (mean 76% MSO, SEM ±0.83). To test whether slight TMS intensity differences at each target, due to E-field modeling, could account for differences across targets observed, we calculated the correlation of early TEP amplitude and stimulation intensity for each individual. There was no association between stimulation intensity and TEP amplitude (mean R=0.24, Fig. S5).

2.4. Electroencephalography

EEG was recorded using a 64-channel TMS-compatible amplifier (ActiCHamp Plus, Brain Products GmbH, Germany) with a 25 kHz sampling rate. Slim, freely rotatable, active electrodes (actiCAP slim, Brain Products GmbH, Germany) were used in a standard montage labeled according to the

extended 10-20 international system. EEG data were online referenced to the 'Cz' electrode and recorded using BrainVision Recorder software (Brain Products GmbH, Germany). Impedance at all electrodes were generally kept below 5 kΩ and monitored at regular intervals throughout each session. Noise masking and earmuffs, as described in detail previously (18), were applied to reduce off-target sensory effects.

2.4.1. Preprocessing of TMS-EEG data

TMS-EEG preprocessing was performed with version 2 of the fully automated AARATEP pipeline (34) (Fig. 1D). Epochs were extracted from 800 ms before to 1000 ms after each TMS pulse. Data between 2 ms before to 12 ms after each pulse were replaced with values interpolated by autoregressive extrapolation and blending (34), downsampled to 1 kHz, and baseline-corrected based on mean values between 500 to 10 ms before the pulse. Epochs were then high-pass filtered above 1 Hz with a modified filtering approach to reduce the spread of pulse-related artifact into baseline time periods. Bad channels were rejected via quantified noise thresholds and replaced with spatially interpolated values. Eye blink artifacts were attenuated by a dedicated round of independent component analysis (ICA) and eye-specific component labeling and rejection using ICLabel (35), a modification from the original AARATEP pipeline introduced in version 2. Various non-neuronal noise sources were attenuated with SOUND (36). Decay artifacts were reduced via a specialized decay fitting and removal procedure (34). Line noise was attenuated with a bandstop filter between 58-62 Hz. Additional artifacts were attenuated with a second stage of ICA and ICLabel labeling and rejection, with rejection criteria targeted at removing any clearly non-neural signals. Data were again interpolated between -2 and 12 ms with autoregressive extrapolation and blending, low-pass filtered below 100 Hz, and average re-referenced. For complete details of the pipeline implementation, see (34) and source code at github.com/chriscline/AARATEPPipeline.

2.4.2. Extraction of early TEP and artifact amplitudes

Our goal was to characterize the local TMS-evoked neural responses and muscle artifacts across the dlPFC. To do so, we computed two measures: 1) the *early TEP*, defined as the min-to-max amplitude within 20 to 50 ms after the TMS pulse; and 2) *early artifact*, induced primarily by local muscle activation (19), and computed as the maximal amplitude from 12-20 ms from the minimally processed (after epoching and baseline correction) data, in dBμV. We focused on the early time window of the TEP, which encompasses the 'P20' and the 'N40' complexes (5,37,38), because 1) there is evidence for the neural basis of the early TEP components (39,40); 2) it has been well-

characterized by other groups (5,37,38); and 3) off-target sensory confounds are more prominent in the later (>100 ms) components (16–18,41–43). Because the timing of the P20 and N40 are variable across locations and subjects, we simplified and quantified the min-to-max amplitude across the time window that captures both peaks. For both *early TEP* and *early artifact* measures, a region of interest (ROI) consisting of six left prefrontal electrodes (F5, F3, F1, FC5, FC3, FC1) was used (Fig. 1F). These electrodes were chosen to broadly cover the dlPFC. Trial-averaged TEPs were calculated with a 10% trimmed mean to prevent a small number of extreme trials from dominating results.

2.4.3. Statistical analyses of early TEPs and artifacts

To test the effect of TMS location and coil orientation, we performed separate two-way repeated-measures analyses of variance (rmANOVAs; factors: stimulation location and coil angle) with Geisser-Greenhouse correction for the early TEP and artifact amplitudes (Fig. 2C, G). Normality was evaluated using the Shapiro–Wilk test (QQ plots in Fig. S3). To further explore how stimulation location affected the early TEPs and early artifacts, we divided the targets into anterior-posterior (targets t1-4) and the medial-lateral (targets t6, t2 and t5) axes (Fig. 2D, E, H and I). For early TEPs and artifacts, we conducted separate paired t-tests for posterior-to-anterior (e.g. t1 versus t4) and medial-lateral (e.g. t6 versus t5) divisions. Then, to better understand how TMS-evoked artifacts relate to early TEPs, targets were categorized into those with low artifact (t1, t2 and t6) and high artifact (t3, t4 and t5) based on a median split of averaged artifact amplitudes. The early TEPs for low versus high artifact targets were compared using a two-tailed paired t-test (Fig. 2J). To understand how individualizing the target would affect the early TEP, we retrospectively compared the individual best location / angle to both the group best and targets t3-4 using paired t-tests (Fig. 3C). T-tests were corrected for multiple comparisons with the Holm-Šídák method. To test uniqueness of each target's evoked whole-brain spatio-temporal activations, the difference of each target was statistically compared to all other targets using cluster-based permutation statistics (44) (cluster threshold<0.05 (two-tailed); two-tailed dependent samples t-test with alpha<0.025; 10000 randomizations; time included: 20-50 ms), as implemented in FieldTrip toolbox (45) (Fig. 4D).

3. Results

3.1. Amplitudes of early TEPs and artifacts are sensitive to TMS target location across the dlPFC.

3.1.1. Early TEPs are sensitive to TMS location and there is a target / angle interaction. We compared early TEP amplitude across targets and angles using a two-way rmANOVA. We found a main effect of target location on early TEPs ($F_{2.69,40.36}$=4.45, P=0.011) but not coil angle ($F_{1,15}$= 1.94, P=0.18; Fig. 2C). We observed a significant interaction of stimulation location and coil angle on early TEPs ($F_{3.60,54.00}$=2.98, P=0.031). Target t6 with 90° coil angle produced the largest early TEPs on group level. Since the main effect of coil angle was non-significant, for further TEP analyses we focus here on 45° angle conditions (results for the 90° coil angle are shown in Supplementary Material).

3.1.2. Posteromedial targets produce larger early TEPs than anterolateral targets. As a follow-up analysis, we asked whether moving the coil along anterior-posterior and medial-lateral axes would produce different TEP amplitudes. The most posterior (t1) and most anterior (t4) targets had significantly different early TEP amplitudes (t_{15}=3.38, P=0.017; Fig. 2D). The most medial (t6) and most lateral (t5) targets also were significantly different in early TEP amplitudes (t_{15}=2.98, P=0.028; Fig. 2E).

3.1.3. Artifacts are sensitive to TMS location but not coil angle. We next explored the effect of early artifacts across dlPFC targets and coil angles (Fig. 2G). We observed a strong main effect of target location on artifacts (two-way rmANOVA, $F_{3.76,56.34}$=27.73, P<0.0001), no main effect of coil angle ($F_{1,15}$= 0.85, P=0.37), and no interaction between location and coil angle ($F_{2.85,42.77}$=0.77, P=0.51). Since the effect of coil angle was non-significant, for further artifact analyses we here focus on 45° angle conditions (results for the 90° coil angle are shown in Supplementary Material).

3.1.4. Posteromedial targets produce smaller artifacts than anterolateral targets. As a follow-up analysis, we asked whether moving the coil along anterior-posterior and medial-lateral axes produced different amounts of artifact. We found that the most posterior (t1) and most anterior (t4) targets had significantly different artifacts (t_{15}=5.88, P=0.00015; Fig. 2H). The most medial (t6) and most lateral (t5) targets also differed (t_{15}=2.91, P=0.028; Fig. 2I), with the most lateral exhibiting larger artifacts.

3.1.5. Targets with smaller artifacts produce larger TEPs. To further understand the relationship between early artifact and TEP strength, which could inform online TEP optimization, we compared early TEP amplitudes between large-artifact and small-artifact targets. After performing a median

split (see Methods), targets with small artifacts produced larger early TEPs than targets with large artifacts (t_{15}=2.22, P=0.042; Fig. 2J).

In summary, within the dlPFC 1) early TEPs and artifacts were sensitive to target location with location / angle interactions and 2) posterior and medial targets produced larger early TEPs and smaller artifacts compared to anterior and lateral targets.

3.2. Retrospectively personalized dlPFC target selection maximizes the early TEP.

It is unknown whether individually optimizing the dlPFC early TEP in real-time can improve signal quality. In order to simulate this individualized approach, we compared the target / angle combination that produced the strongest early TEP in each individual to the group best combination. We observed high variability across subjects – only four out of 16 subjects had an individual optimal early TEP combination that matched the group-level best (target t6, 90° coil angle; Fig. 3A and B). We compared the individual optimized early TEPs to group optimized target (t6, 90° coil angle), and standard clinical targets (target t3 close to BA9 definition (27) and target t4 with activity which is most negatively correlated to the sgACC (25)). The individual optimized approach produced larger early TEPs compared to the group-best (t_{15}=4.65, P=0.00031), target t4 (t_{15}=7.42, P<0.0001) and target t3 (t_{15}=9.05, P<0.0001; Fig. 3C). Group best target produced 102% larger early TEPs compared to the standard clinical targets. Individually-selected optimal early TEPs demonstrated a 36% increase over group best and 174% over the average of standard clinical targets (in μV values; Fig. 3C). In summary, these results suggest that target / angle personalization may enhance the strength of early TEPs.

3.3 Differences in brainwide neural responses across dlPFC stimulation targets

As an exploratory analysis to characterize stimulation target specificity of the brainwide neural response to TMS with fewer assumptions about relevant electrode locations, we compared the TEP response at each target (t1-t6) to the average responses to all other targets (45° coil angle for all). Butterfly plots and topographies of the TEPs for these conditions are shown in Fig 4B-C. Cluster-based permutation testing of the differences between each of these sites and the average responses at all other sites between 20-50 ms revealed significant differences, with topographies of difference t-values and electrodes belonging to suprathreshold clusters shown in Fig 4D. Significant target-specific activations were found for each target except t5, suggesting that brainwide spatiotemporal patterns in the 20-50 ms response window were sensitive to coil location.

4. Discussion

Summary of findings. In the current study we sought to better understand how the early TEP, a causal measure of cortical excitability, varies across TMS coil target locations and coil angles when stimulating the dlPFC. Our findings were as follows: (1) Early TEPs and artifacts varied significantly as a function of dlPFC target. Specifically, lateral and anterior targets produced smaller early TEPs and larger artifacts, whereas medial and posterior targets produced larger early TEPs and smaller artifacts. The group best target yielded 102% larger early TEP compared to standard targets. This analysis also revealed that target location interacts with coil angle for early TEPs; (2) Individual offline optimization of target and angle enhanced the early TEP by 36%; (3) All targets except the most lateral target (t5) showed different whole-brain spatio-temporal responses in the early TEP time window compared to the other targets. In summary, the study furthers our understanding of this causal metric of cortical excitability across the dlPFC. This work suggests that effects of rTMS treatment could be confidently monitored with early TEPs in the posterior-medial aspects of the dlPFC and that a personalized, real-time approach to targeting may further improve the signal quality of the early TEP.

Early TEP as a function of dlPFC target and coil angle. To date, little is known about how noninvasive brain measurements, including the early TEP, vary across stimulation targets and coil angles within the dlPFC. This information is critical to effectively monitor the neural effects of rTMS treatment. Here, we observed a large variability in early TEP strength across different targets and coil orientations. Specifically, early TEPs were up to two times larger in posterior-medial regions compared to anterior-lateral regions, and in regions where early TEPs were larger, early artifacts were smaller (Fig 2). These results may be due to the fact that the large frontalis muscle is typically located in closer proximity with anterior targets, whereas the temporalis muscle is located close to the lateral targets. It is worth noting though that there is large inter-subject variability with respect to the muscle distribution, and on an individual level the relationship between early TEPs and muscle artifact was only moderately inversely correlated (Fig. S6). Whether this difference in early TEP variability across targets represents differences in true cortical excitability or strength differences from the muscle artifact masking early TEPs is unclear. Furthermore, although we do not find evidence for a main effect of coil angle on the early TEP or artifact, we do observe an interaction of target with coil angle on early TEPs. Further work is needed to explore how coil angle should be modified based on target location to optimize early TEPs. Future studies should also focus on relating differences in early TEPs across target and angle to differences in anatomical structure

(e.g. gyral folding) and downstream functional networks to enhance its biological validity. Early TEPs have been linked to GABAergic inhibition, and related to both depression (46) and treatment response to rTMS (2,3). Multiple lines of evidence also suggest that early TEPs have intracranial neural correlates (39,40). However, more work is needed to better understand the relationship between the strength of early TEPs to downstream functional brain networks. Before testing clinical utility of early TEPs, the optimized TEPs need to be evaluated for reliability across multiple visits and sensitivity to the neural effects of rTMS, most importantly in patients. In summary, this work sheds light on the dlPFC subregions that can be confidently monitored with large early TEPs and emphasizes the need for future studies on the biological validity of early TEPs.

Personalized treatment monitoring with early TEPs. This work demonstrates promise utilizing a personalized approach for improving the early TEP signal. Real-time early TEP optimization is an important next step for ensuring high quality early TEPs during experiments or treatment. Retrospectively, we observed a 102% boost in early TEP amplitude when selecting the group best target (target t6, 90° coil angle), and additional 36% boost when selecting the best target and angle for each individual (Fig 3C). It is worth noting that the final boost in early TEP strength by personalizing is likely larger than 36%. This is because the early TEP can be personalized across more dimensions than tested here, including spatial location down to the millimeter, angle down to the degree, and intensity. We suggest that a similar or stronger boost in early TEP signal strength could thus be achieved in real-time. This online approach to optimize early TEPs has been shown to be feasible, at least with a custom-made TMS setup and stimulating pre-supplementary motor region and sufficient time for experimentation (47). This personalized approach can be used in the future to monitor the neural changes during and after neuromodulatory as well as non-neuromodulatory treatments. But before doing so, future work should validate these retrospective individualized findings prospectively using real-time online optimization. For implementation, it will be essential to have a fully automated approach that can be completed in a short experimental window (<20 minutes). Future work will also focus on if any additional boost can come from refining targets, coil angles, and intensity outside of those tested here. Another important consideration in future studies will be the balance between the extra experimental time needed to optimize these early TEPs and the strength of improvement. If the optimization protocol produces only a modest boost, for some studies utilizing the group-best (target t6, 90° coil angle) target may yield strong enough results. For others, only minor online optimization with granular adjustments in target, angle, and intensity may be worthwhile.

Limitations and future directions. Several limitations are worth discussing. First, our choice of brain targets was driven by equidistant sampling of the middle frontal gyrus as well as the desire to probe the anterior-posterior and medial-lateral directions. Future work should follow up on these findings and include the following investigations: Analysis of the inter-target variability of the early TEP 1) at finer spatial resolution and 2) at additional anterior-medial targets. A second limitation is that we only used two coil angles. Future work should explore how other coil angles affect the early TEP. Developing online algorithms to fully automate target / angle search space within and outside of the dlPFC could prove valuable but is outside the scope of this work. Third, it is worth considering the influence of our E-field modeling approach on the results, as offline E-field modeling has its own limitations. Although our results suggest that absolute intensity differences did not contribute significantly to early TEP strength (Fig. S5), E-field modeling could influence the effective intensities used to probe different targets (48,49). In the future as these models continue to improve, it is worth re-examining these targets with more sophisticated E-field matching.

The early TEP time window was primarily chosen based on previous reports of neurophysiological effects of TMS in this time window (50) and potential clinical relevance (2,3,46). In addition, this time window was chosen to avoid off-target sensory components that are usually reported between 100 and 200 ms (18). It is worth noting that there are potential sensory responses even in this 20-50 ms time window (51–57), as auditory stimuli can elicit neural responses in EEG within 10 to 60 ms after stimulus onset (for a review, see (58)). However, the early TEP has been shown to be unaffected by sensory suppression techniques, supporting the notion that sensory contributions during this time period is likely minimal (17,18). Further, we implemented auditory suppression techniques (18) and our GMFA time series (Fig. S7) support that condition-specific differences in the 100-200 ms window were not accompanied by similar patterns in the early TEP time window. For all these reasons, we feel that it is unlikely that the early TEP reported on here is sensory in nature.

Finally, it is worth considering the implications of the study with respect to rTMS treatment. High signal strength of the early TEP says little about the optimal treatment targets within the dlPFC. Multiple dlPFC treatment targets for depression have been proposed based on symptom profiles (59) and network activation (25,29), and the objective of the current study was simply to determine which of these targets could be sampled with early TEPs at high signal quality. Future work is needed to explore the relationship between the optimized early TEP target / angle and optimized rTMS treatment.

Conclusions. This study characterized the early TEP across brain targets and angles within the dlPFC. We observed clear group-level trends, including posterior and medial targets resulting in larger early TEPs and smaller artifacts compared to anterior and lateral targets. The best group-level target resulted in 102% larger early TEPs compared to other standard targets. Consistent with previous reports, we observed high variability across subjects, and our data suggests that this variability can be used to personalize and optimize the early TEP on an individual subject basis, leading to additional >30% boost in signal. In summary, this study furthers our understanding of cortical excitability across the dlPFC. This work suggests that effects of TMS treatment could be confidently monitored with early TEPs in the posterior-medial aspects of the dlPFC and a personalized approach to this monitoring may further improve its signal strength.

Acknowledgements.

We extend our deep gratitude to all of our research participants. We would also like to acknowledge the generous contributions of the members of the Personalized Neurotherapeutics Laboratory for helpful feedback on the manuscript and throughout the course of the study. This research was supported by the National Institute of Mental Health under award number R01MH126639, R01MH129018, and a Burroughs Wellcome Fund Career Award for Medical Scientists (CJK). JG was supported by personal grants from Orion Research Foundation and the Finnish Medical Foundation. JMR was supported by the Department of Veterans Affairs Office of Academic Affiliations Advanced Fellowship Program in Mental Illness Research and Treatment, the Medical Research Service of the Veterans Affairs Palo Alto Health Care System and the Department of Veterans Affairs Sierra-Pacific Data Science Fellowship.

Declaration of Interest.

Corey Keller holds equity in Alto Neuroscience, Inc. All other authors have nothing to disclose.

Figures and Legends

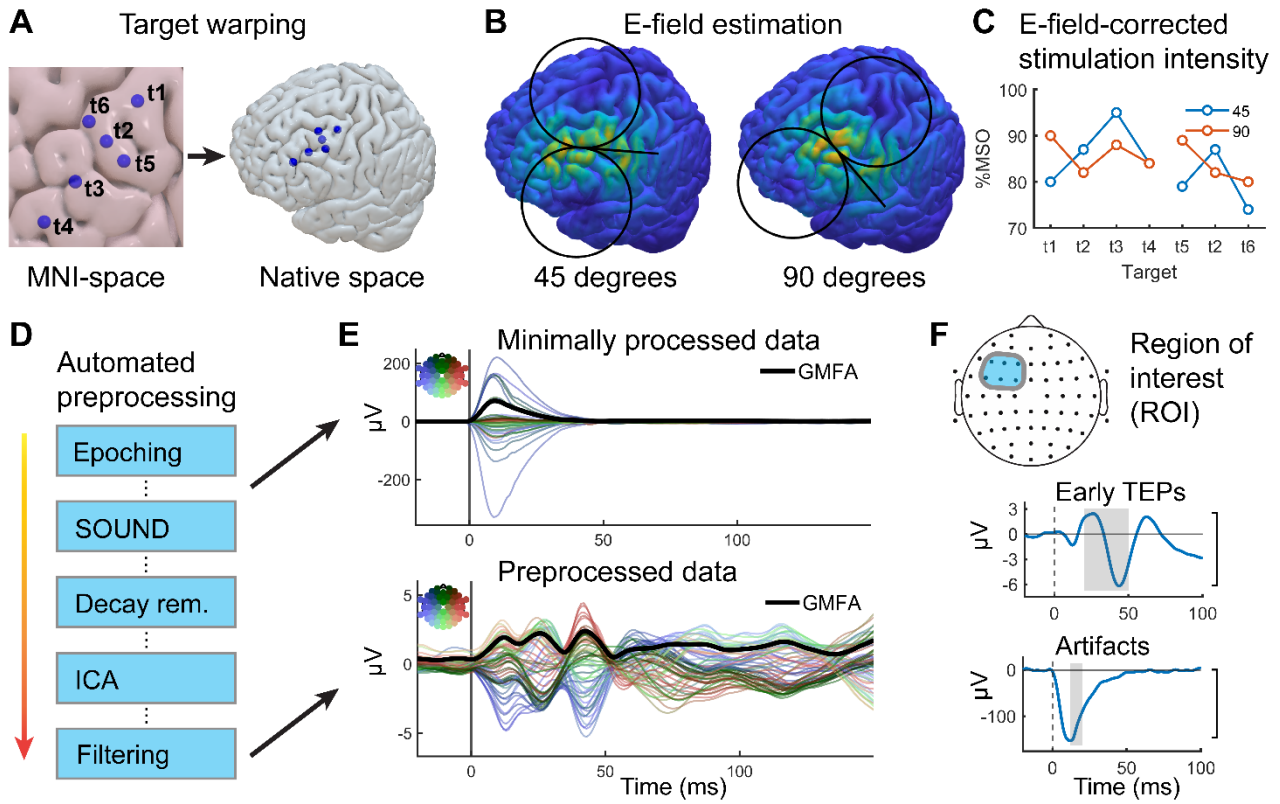

Figure 1 - Study schematic. A) Targets for single pulse TMS within the dlPFC in MNI and native space. Stimulation targets were warped to individual space for each subject. B) Before the TMS-EEG session, maximal E-field was calculated for each target / angle combination. The stimulation intensity was adjusted for each target / angle combination so that the maximal induced E-field was the same in the dlPFC as compared to the intensity of 120% rMT in the primary motor cortex. Shown are E-fields for one target with 45° (left) and 90° (right) angles in a representative subject. C) Adjusted stimulation intensities for each target and angle in a representative subject. D) The data were preprocessed using a fully automatized preprocessing pipeline, described in detail in (34). For each condition, artifact amplitude was quantified before artifact removal (SOUND). E) Example butterfly plots (one target / angle condition, 150 trials, N=1 subject). F) For TEP analyses, an ROI consisting of six prefrontal electrodes (F5, F3, F1, FC5, FC3, FC1) was used (top). Peak-to-peak amplitudes of early TEPs (middle) and maximal values of artifacts (bottom) were quantified. One condition is shown for a representative subject. Brackets denote the amplitude of early TEP and artifact.

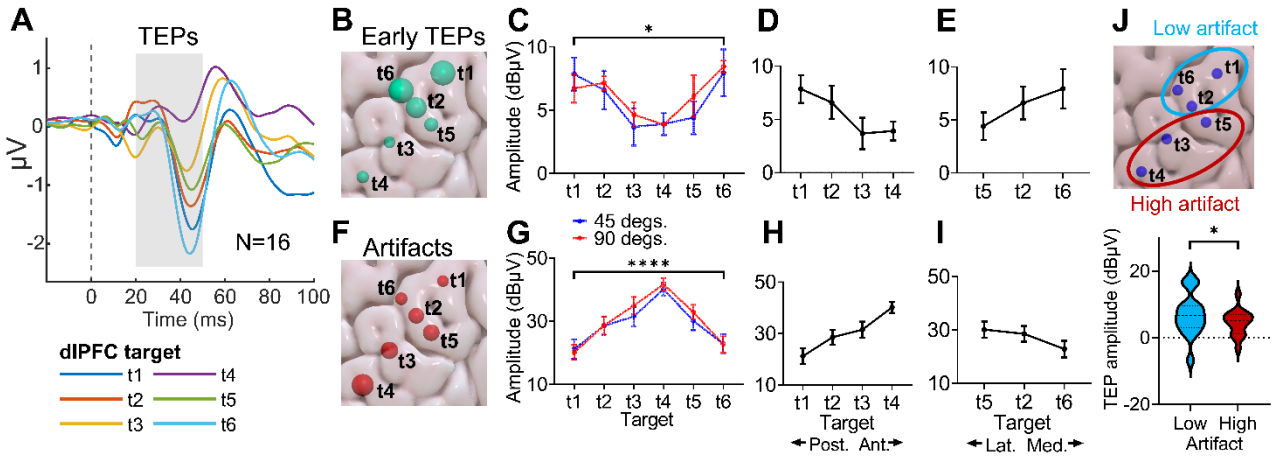

Figure 2 - Early TEPs and artifacts are sensitive to TMS target within the dlPFC. A) Grand average (N=16) early TEPs for each stimulation target (ROI: left prefrontal cortex, 45° coil angle). Grey area represents the time window (20 to 50 ms) in which the early TEP amplitude is calculated. B-E) Relationship between stimulation targets and early TEPs (45° coil angle). In panel B, marker size represents the early TEP across subjects. F-I) Same as B-E but for artifacts. J) Relationship between artifact magnitude and early TEP amplitude. *In C-E and G-I lines represent mean ± SEM (N=16). Lines in D and E are shown for two-way rmANOVA interaction interpretation. *P<0.05 (in J paired t-test corrected for multiple comparisons, N=16; in C a significant main effect for stimulation target and interaction of target and coil angle in the two-way rmANOVA, N=16). ****P<0.0001 (significant main effect for stimulation target in the two-way rmANOVA, N=16).*

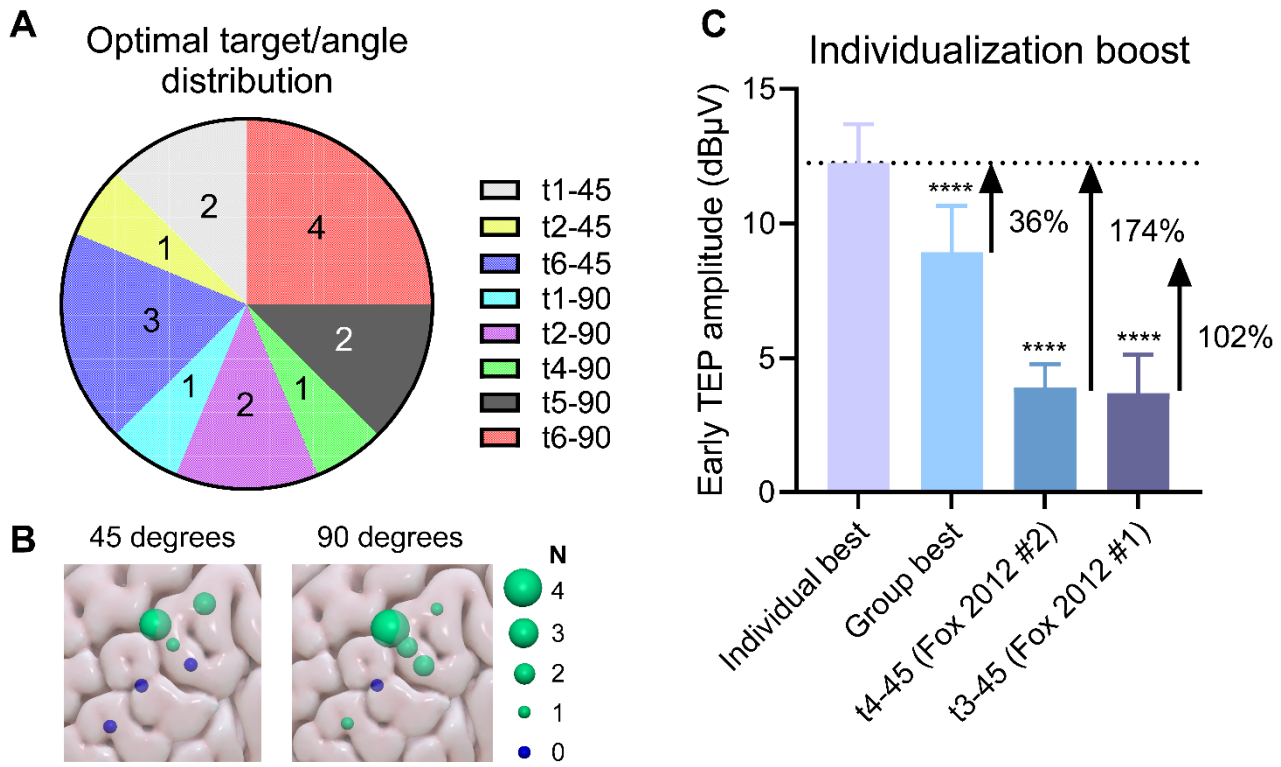

Figure 3 - Personalized target selection maximizes the early TEP. A) Pie chart of individual best target / angle combinations (the combination that produced largest early TEPs). Number in each slice represents the number of subjects having a given target / angle combination as their optimal. B) Number of subjects with each target location as their optimal, shown on cortical surface. C) Early TEP as a function of different targets. 'Group best' early TEP is larger than the early TEP responses to targets negatively correlated to sgACC (t4-45, which has the same coordinates as suggested in Fox *et al*. 2012) and t3-45 (which is located between 'BA9 Definition' of Rajkowska *et al*. 1995 and a another target with activity negatively correlated to sgACC (25)). The individual best target yields significantly larger early TEPs compared to either group best or t4/t3 targets. Boost percentages are calculated using µV values. *In C bars represent mean ± SEM (N=16). ****P<0.0001 (Holm-Šídák's multiple comparisons test, compared to 'Individual best').*

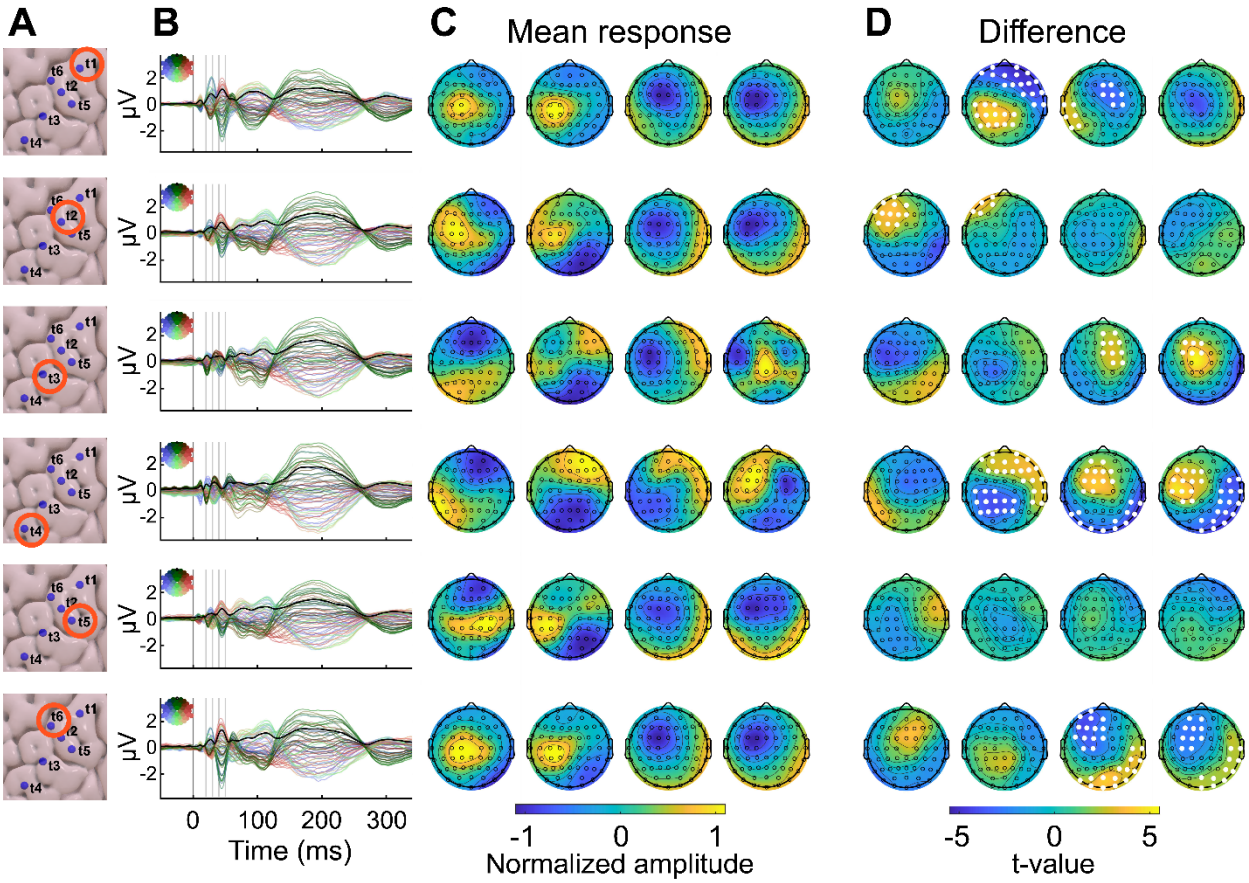

Figure 4 - Stimulation of dlPFC targets elicit unique whole-brain spatio-temporal activation patterns. A-C) Group (N=16) location (A), butterfly plot (B), and scalp topographies (C) for all targets (all at 45° angle). D) Spatio-temporal differences between a selected target and all other targets, as implemented by cluster-based permutation testing. Electrodes belonging to statistically significant clusters are highlighted as white dots (*P<0.001*).

References

1. Mutz J, Edgcumbe DR, Brunoni AR, Fu CHY (2018): Efficacy and acceptability of non-invasive brain stimulation for the treatment of adult unipolar and bipolar depression: A systematic review and meta-analysis of randomised sham-controlled trials. *Neurosci Biobehav Rev* 92: 291–303.
2. Eshel N, Keller CJ, Wu W, Jiang J, Mills-Finnerty C, Huemer J, *et al.* (2020): Global connectivity and local excitability changes underlie antidepressant effects of repetitive transcranial magnetic stimulation. *Neuropsychopharmacol Off Publ Am Coll Neuropsychopharmacol* 45: 1018–1025.
3. Voineskos D, Blumberger DM, Rogasch NC, Zomorrodi R, Farzan F, Foussias G, *et al.* (2021): Neurophysiological effects of repetitive transcranial magnetic stimulation (rTMS) in treatment resistant depression. *Clin Neurophysiol Off J Int Fed Clin Neurophysiol* 132: 2306–2316.
4. Ferrarelli F, Phillips ML (2021): Examining and Modulating Neural Circuits in Psychiatric Disorders With Transcranial Magnetic Stimulation and Electroencephalography: Present Practices and Future Developments. *Am J Psychiatry* 178: 400–413.
5. Lioumis P, Kicić D, Savolainen P, Mäkelä JP, Kähkönen S (2009): Reproducibility of TMS-Evoked EEG responses. *Hum Brain Mapp* 30: 1387–1396.
6. Massimini M, Ferrarelli F, Esser SK, Riedner BA, Huber R, Murphy M, *et al.* (2007): Triggering sleep slow waves by transcranial magnetic stimulation. *Proc Natl Acad Sci U S A* 104: 8496–8501.
7. Bergmann TO, Mölle M, Schmidt MA, Lindner C, Marshall L, Born J, Siebner HR (2012): EEG-guided transcranial magnetic stimulation reveals rapid shifts in motor cortical excitability during the human sleep slow oscillation. *J Neurosci Off J Soc Neurosci* 32: 243–253.
8. Casarotto S, Canali P, Rosanova M, Pigorini A, Fecchio M, Mariotti M, *et al.* (2013): Assessing the effects of electroconvulsive therapy on cortical excitability by means of transcranial magnetic stimulation and electroencephalography. *Brain Topogr* 26: 326–337.
9. Gosseries O, Thibaut A, Boly M, Rosanova M, Massimini M, Laureys S (2014): Assessing consciousness in coma and related states using transcranial magnetic stimulation combined with electroencephalography. *Ann Fr Anesth Reanim* 33: 65–71.
10. Mutanen T, Mäki H, Ilmoniemi RJ (2013): The effect of stimulus parameters on TMS-EEG muscle artifacts. *Brain Stimulat* 6: 371–376.
11. Kerwin LJ, Keller CJ, Wu W, Narayan M, Etkin A (2018): Test-retest reliability of transcranial magnetic stimulation EEG evoked potentials. *Brain Stimulat* 11: 536–544.

12. Rogasch NC, Thomson RH, Daskalakis ZJ, Fitzgerald PB (2013): Short-latency artifacts associated with concurrent TMS-EEG. *Brain Stimulat* 6: 868–876.
13. Rogasch NC, Thomson RH, Farzan F, Fitzgibbon BM, Bailey NW, Hernandez-Pavon JC, *et al.* (2014): Removing artefacts from TMS-EEG recordings using independent component analysis: importance for assessing prefrontal and motor cortex network properties. *NeuroImage* 101: 425–439.
14. Casarotto S, Fecchio M, Rosanova M, Varone G, D'Ambrosio S, Sarasso S, *et al.* (2022): The rt-TEP tool: real-time visualization of TMS-Evoked Potentials to maximize cortical activation and minimize artifacts. *J Neurosci Methods* 370: 109486.
15. Darmani G, Bergmann TO, Zipser C, Baur D, Müller-Dahlhaus F, Ziemann U (2019): Effects of antiepileptic drugs on cortical excitability in humans: A TMS-EMG and TMS-EEG study. *Hum Brain Mapp* 40: 1276–1289.
16. Biabani M, Fornito A, Mutanen TP, Morrow J, Rogasch NC (2019): Characterizing and minimizing the contribution of sensory inputs to TMS-evoked potentials. *Brain Stimulat* 12: 1537–1552.
17. Ross JM, Ozdemir RA, Lian SJ, Fried PJ, Schmitt EM, Inouye SK, *et al.* (2022): A structured ICA-based process for removing auditory evoked potentials. *Sci Rep* 12: 1391.
18. Ross JM, Sarkar M, Keller CJ (2022): Experimental suppression of transcranial magnetic stimulation-electroencephalography sensory potentials. *Hum Brain Mapp*. https://doi.org/10.1002/hbm.25990
19. Mäki H, Ilmoniemi RJ (2011): Projecting out muscle artifacts from TMS-evoked EEG. *NeuroImage* 54: 2706–2710.
20. Rush AJ, Trivedi MH, Ibrahim HM, Carmody TJ, Arnow B, Klein DN, *et al.* (2003): The 16-Item Quick Inventory of Depressive Symptomatology (QIDS), clinician rating (QIDS-C), and self-report (QIDS-SR): a psychometric evaluation in patients with chronic major depression. *Biol Psychiatry* 54: 573–583.
21. Rossi S, Hallett M, Rossini PM, Pascual-Leone A (2011): Screening questionnaire before TMS: an update. *Clin Neurophysiol Off J Int Fed Clin Neurophysiol* 122: 1686.
22. Rossi S, Hallett M, Rossini PM, Pascual-Leone A (2009): Safety, ethical considerations, and application guidelines for the use of transcranial magnetic stimulation in clinical practice and research. *Clin Neurophysiol* 120: 2008–2039.
23. ter Braack EM, de Vos CC, van Putten MJAM (2015): Masking the Auditory Evoked Potential in TMS-EEG: A Comparison of Various Methods. *Brain Topogr* 28: 520–528.
24. Cash RFH, Weigand A, Zalesky A, Siddiqi SH, Downar J, Fitzgerald PB, Fox MD (2021): Using

Brain Imaging to Improve Spatial Targeting of Transcranial Magnetic Stimulation for Depression. *Biol Psychiatry* 90: 689–700.

25. Fox MD, Buckner RL, White MP, Greicius MD, Pascual-Leone A (2012): Efficacy of transcranial magnetic stimulation targets for depression is related to intrinsic functional connectivity with the subgenual cingulate. *Biol Psychiatry* 72: 595–603.
26. Herwig U, Lampe Y, Juengling FD, Wunderlich A, Walter H, Spitzer M, Schönfeldt-Lecuona C (2003): Add-on rTMS for treatment of depression: a pilot study using stereotaxic coil-navigation according to PET data. *J Psychiatr Res* 37: 267–275.
27. Rajkowska G, Goldman-Rakic PS (1995): Cytoarchitectonic definition of prefrontal areas in the normal human cortex: II. Variability in locations of areas 9 and 46 and relationship to the Talairach Coordinate System. *Cereb Cortex N Y N 1991* 5: 323–337.
28. Herbsman T, Avery D, Ramsey D, Holtzheimer P, Wadjik C, Hardaway F, *et al.* (2009): More lateral and anterior prefrontal coil location is associated with better repetitive transcranial magnetic stimulation antidepressant response. *Biol Psychiatry* 66: 509–515.
29. Weigand A, Horn A, Caballero R, Cooke D, Stern AP, Taylor SF, *et al.* (2018): Prospective Validation That Subgenual Connectivity Predicts Antidepressant Efficacy of Transcranial Magnetic Stimulation Sites. *Biol Psychiatry* 84: 28–37.
30. Huang C-C, Rolls ET, Feng J, Lin C-P (2022): An extended Human Connectome Project multimodal parcellation atlas of the human cortex and subcortical areas. *Brain Struct Funct* 227: 763–778.
31. Nielsen JD, Madsen KH, Puonti O, Siebner HR, Bauer C, Madsen CG, *et al.* (2018): Automatic skull segmentation from MR images for realistic volume conductor models of the head: Assessment of the state-of-the-art. *NeuroImage* 174: 587–598.
32. Thielscher A, Antunes A, Saturnino GB (2015): Field modeling for transcranial magnetic stimulation: A useful tool to understand the physiological effects of TMS? *Annu Int Conf IEEE Eng Med Biol Soc IEEE Eng Med Biol Soc Annu Int Conf* 2015: 222–225.
33. Caulfield KA, Li X, George MS (2021): Four electric field modeling methods of Dosing Prefrontal Transcranial Magnetic Stimulation (TMS): Introducing APEX MT dosimetry. *Brain Stimulat* 14: 1032–1034.
34. Cline CC, Lucas MV, Sun Y, Menezes M, Etkin A (2021): Advanced Artifact Removal for Automated TMS-EEG Data Processing. *2021 10th International IEEE/EMBS Conference on Neural Engineering (NER)* 1039–1042.
35. Pion-Tonachini L, Kreutz-Delgado K, Makeig S (2019): ICLabel: An automated electroencephalographic independent component classifier, dataset, and website.

NeuroImage 198: 181–197.

36. Mutanen TP, Metsomaa J, Liljander S, Ilmoniemi RJ (2018): Automatic and robust noise suppression in EEG and MEG: The SOUND algorithm. *NeuroImage* 166: 135–151.
37. Kähkönen S, Komssi S, Wilenius J, Ilmoniemi RJ (2005): Prefrontal transcranial magnetic stimulation produces intensity-dependent EEG responses in humans. *NeuroImage* 24: 955–960.
38. Tremblay S, Rogasch NC, Premoli I, Blumberger DM, Casarotto S, Chen R, *et al.* (2019): Clinical utility and prospective of TMS-EEG. *Clin Neurophysiol Off J Int Fed Clin Neurophysiol* 130: 802–844.
39. Huang Y, Hajnal B, Entz L, Fabó D, Herrero JL, Mehta AD, Keller CJ (2019): Intracortical Dynamics Underlying Repetitive Stimulation Predicts Changes in Network Connectivity. *J Neurosci Off J Soc Neurosci* 39: 6122–6135.
40. Keller CJ, Huang Y, Herrero JL, Fini ME, Du V, Lado FA, *et al.* (2018): Induction and Quantification of Excitability Changes in Human Cortical Networks. *J Neurosci Off J Soc Neurosci* 38: 5384–5398.
41. Freedberg M, Reeves JA, Hussain SJ, Zaghloul KA, Wassermann EM (2020): Identifying site- and stimulation-specific TMS-evoked EEG potentials using a quantitative cosine similarity metric. *PloS One* 15: e0216185.
42. Rocchi L, Di Santo A, Brown K, Ibáñez J, Casula E, Rawji V, *et al.* (2021): Disentangling EEG responses to TMS due to cortical and peripheral activations. *Brain Stimulat* 14: 4–18.
43. Conde V, Tomasevic L, Akopian I, Stanek K, Saturnino GB, Thielscher A, *et al.* (2019): The non-transcranial TMS-evoked potential is an inherent source of ambiguity in TMS-EEG studies. *NeuroImage* 185: 300–312.
44. Maris E, Oostenveld R (2007): Nonparametric statistical testing of EEG- and MEG-data. *J Neurosci Methods* 164: 177–190.
45. Oostenveld R, Fries P, Maris E, Schoffelen J-M (2011): FieldTrip: Open source software for advanced analysis of MEG, EEG, and invasive electrophysiological data. *Comput Intell Neurosci* 2011: 156869.
46. Voineskos D, Blumberger DM, Zomorrodi R, Rogasch NC, Farzan F, Foussias G, *et al.* (2019): Altered Transcranial Magnetic Stimulation-Electroencephalographic Markers of Inhibition and Excitation in the Dorsolateral Prefrontal Cortex in Major Depressive Disorder. *Biol Psychiatry* 85: 477–486.
47. Tervo AE, Nieminen JO, Lioumis P, Metsomaa J, Souza VH, Sinisalo H, *et al.* (2022): Closed-loop optimization of transcranial magnetic stimulation with electroencephalography

feedback. *Brain Stimulat* 15: 523–531.

48. Saturnino GB, Madsen KH, Thielscher A (2021): Optimizing the electric field strength in multiple targets for multichannel transcranial electric stimulation. *J Neural Eng* 18. https://doi.org/10.1088/1741-2552/abca15
49. Drakaki M, Mathiesen C, Siebner HR, Madsen K, Thielscher A (2022): Database of 25 validated coil models for electric field simulations for TMS. *Brain Stimulat* 15: 697–706.
50. Esser SK, Huber R, Massimini M, Peterson MJ, Ferrarelli F, Tononi G (2006): A direct demonstration of cortical LTP in humans: a combined TMS/EEG study. *Brain Res Bull* 69: 86–94.
51. A novel EEG paradigm to simultaneously and rapidly assess the functioning of auditory and visual pathways - PubMed (n.d.): Retrieved December 22, 2022, from https://pubmed.ncbi.nlm.nih.gov/31268796/
52. Näätänen R, Picton T (1987): The N1 wave of the human electric and magnetic response to sound: a review and an analysis of the component structure. *Psychophysiology* 24: 375–425.
53. Knight RT, Hillyard SA, Woods DL, Neville HJ (1980): The effects of frontal and temporal-parietal lesions on the auditory evoked potential in man. *Electroencephalogr Clin Neurophysiol* 50: 112–124.
54. Vanni S, Warnking J, Dojat M, Delon-Martin C, Bullier J, Segebarth C (2004): Sequence of pattern onset responses in the human visual areas: an fMRI constrained VEP source analysis. *NeuroImage* 21: 801–817.
55. Davis PA (1939): Effects of acoustic stimuli on the waking human brain. *J Neurophysiol* 2: 494–499.
56. Davis H, Zerlin S (1966): Acoustic relations of the human vertex potential. *J Acoust Soc Am* 39: 109–116.
57. Geisler CD, Frishkopf LS, Rosenblith WA (1958): Extracranial responses to acoustic clicks in man. *Science* 128: 1210–1211.
58. Kappenman ES, Luck SJ (2011): *ERP Components: The Ups and Downs of Brainwave Recordings*. Oxford University Press. https://doi.org/10.1093/oxfordhb/9780195374148.013.0014
59. Fried EI, Nesse RM (2015): Depression is not a consistent syndrome: An investigation of unique symptom patterns in the STAR*D study. *J Affect Disord* 172: 96–102.

Supplementary Material

Analyses of TEPs and artifacts for 90° coil angle

In addition to the analyses for 45° coil angle (see Results), we also conducted similar follow-up analyses for 90° data. We asked whether using the most anterior targets can lead to significantly different early TEP amplitudes than when using the most posterior target. We also asked whether using the most lateral target would lead to different TEP amplitudes compared to the most medial target. The most posterior (t1) and most anterior (t4) targets did not have significantly different early TEP amplitudes (t_{15}=0.85, P=0.65; Fig. S4A). The most medial (t6) and most lateral (t5) targets were not significantly different in early TEP amplitudes (t_{15}=0.85, P=0.65; Fig. S4B) either.

Similarly as for 45° coil angle, we asked whether moving the coil along anterior-posterior and medial-lateral axes would produce differing amounts of artifact with 90° coil angle. We found that the most posterior (t1) and most anterior (t4) targets had significantly different artifacts (t_{15}=10.84, P<0.000001; Fig. S4C). The most medial (t6) and most lateral (t5) targets also differed (t_{15}=4.59, P=0.0011; Fig. S4D), with the most lateral having larger artifacts.

Figures and plotting

MATLAB R2021b (Mathworks, USA) and GraphPad Prism 9 (GraphPad Software, USA) were used for plotting. Stimulation targets (Fig. 1A, Fig. 2-4) were visualized using Surf Ice (https://www.nitrc.org/projects/surfice/). For the butterfly plots and scalp topographies (Fig. 4B and C), the data of each stimulation target was averaged across subjects. Global mean field amplitude (GMFA) was also overlaid on each butterfly plot. For each topographic visualization, the spatial distributions were normalized. All figures were assembled using Adobe Illustrator 2022 (Adobe Inc., USA).

Distances	Point1	Point2	
14.85	t2	t1	a-p
14.85	t3	t2	
14.85	t4	t3	
29.71	t4	t2	
44.56	t4	t1	
15.36	t5	t6	lat-med
17.95	t1	t5	
15.39	t1	t6	
7.68	t2	t5	
7.68	t2	t6	

Supplementary Table 1 - Distances between the stimulation sites (MNI space).

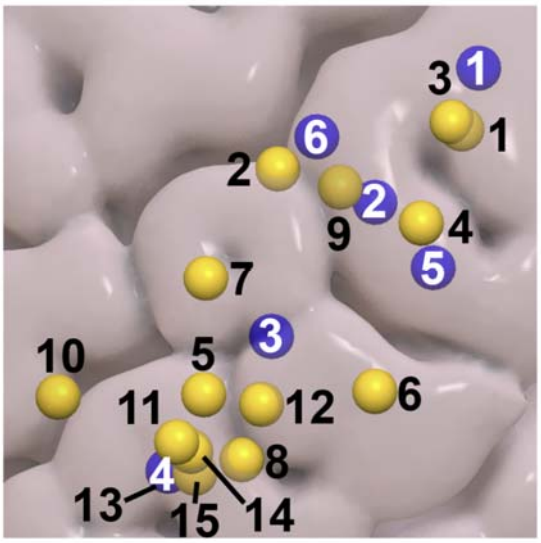

1	5cm average (Fox et al., 2012)
2	5.5cm average (Weigand et al., 2018)
3	Non-responders (Herbsman et al., 2009)
4	Responders (Herbsman et al., 2009)
5	TMS Target (Fitzgerald et al., 2009)
6	TMS Target (Rusjan et al., 2010)
7	BA9 Definiton (Rajkowska et al., 1995)
8	BA46 Definiton (Rajkowska et al., 1995)
9	EEG F3 site (Herwig et al., 2003)
10	EEG F3 site (Okamotu et al., 2004)
11	Beam F3 (Cash et al., 2019)
12	Optimal FC Group Target #1 (Fox et al., 2012)
13	Optimal FC Group Target #2 (Fox et al., 2012)
14	Optimal FC Group Target (Weigand et al., 2018)
15	Optimal FC Group Target (Cash et al., 2019)

Supplementary Figure 1 - Spatial relationship of the targets used in the current paper compared to earlier depression treatment targets (as summarized by Cash et al. 2021 (24)). The treatment target with activity that is most negatively correlated to the sgACC according to Fox at al. 2012 (25) (13 in the figure) has the same MNI coordinates as t4 in the current study. *Blue blobs depict the targets (t1-6) used in the current study, yellow blobs correspond to rTMS depression treatment targets.*

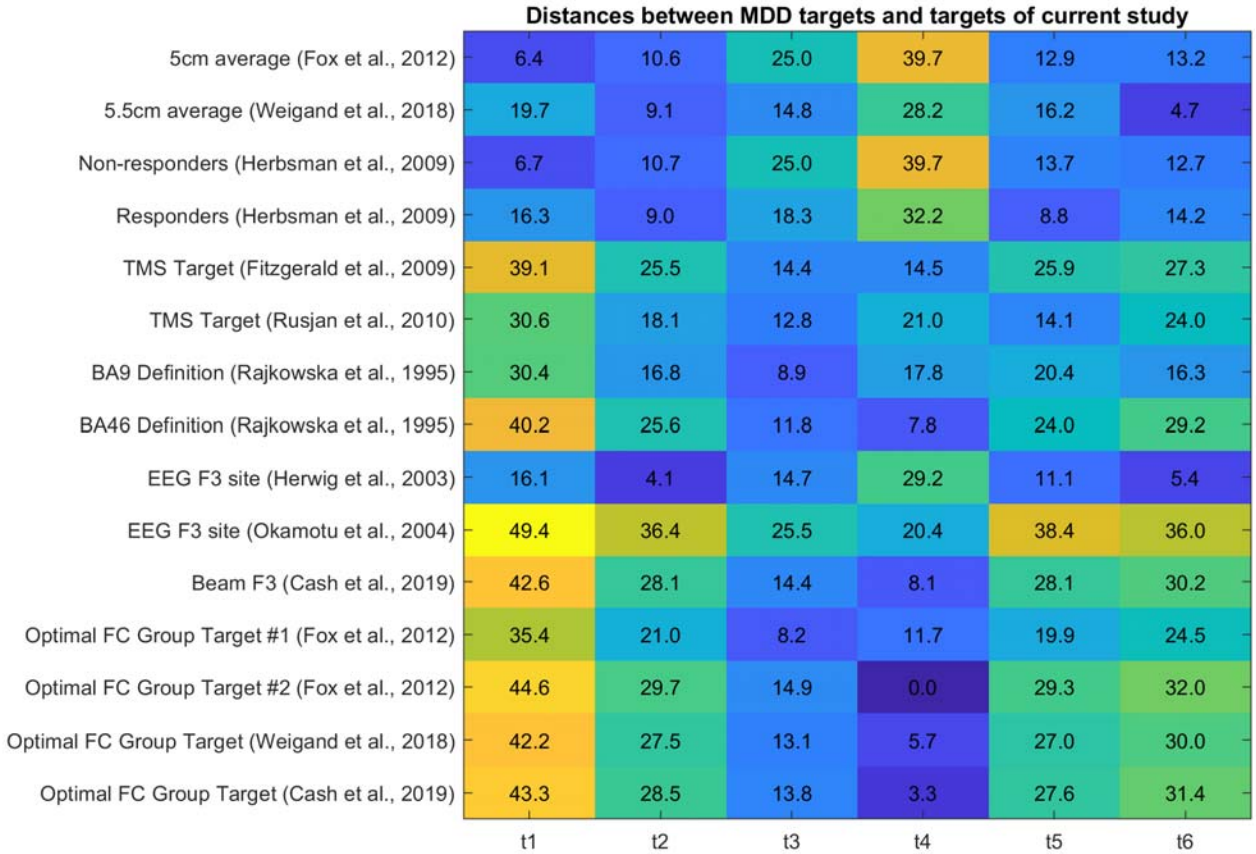

Supplementary Figure 2 - Euclidean distances between the clinical targets (as summarized by Cash et al. 2021 (24)) and the targets of the current study.

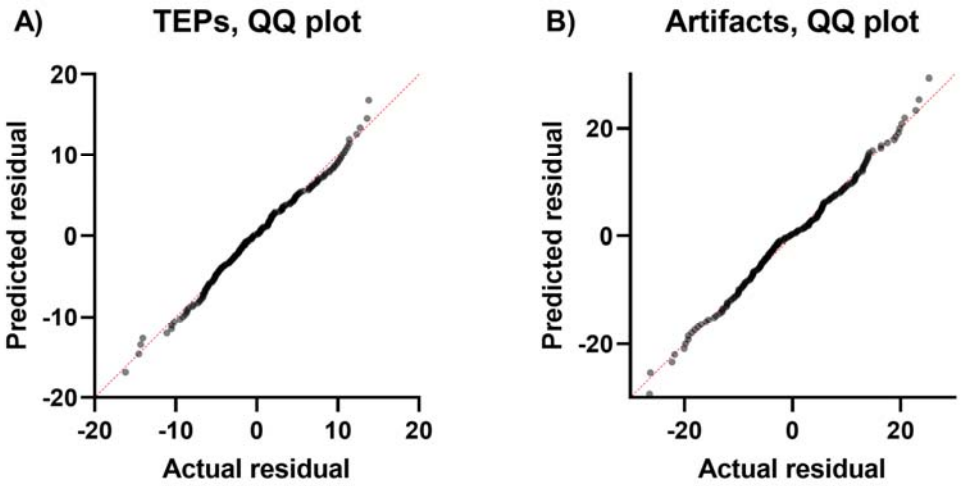

Supplementary Figure 3 - QQ plots for A) early TEP, and B) artifact distributions.

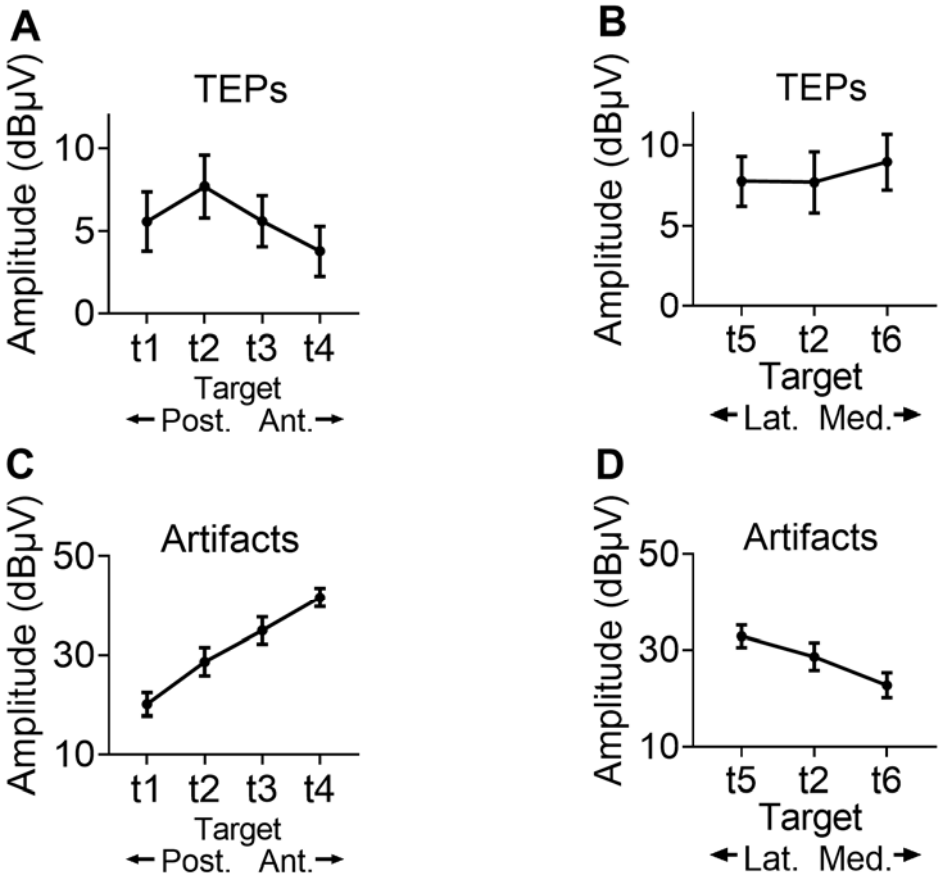

Supplementary Figure 4 - Target-related sensitivity of TEPs and artifacts for 90 degrees coil angle. A-B) Relationship between target (t1-t6, x-axis) and early TEP amplitude with 90 degrees coil angle. C-D) Relationship between stimulation target and muscle artifact with 90 degrees coil angle.

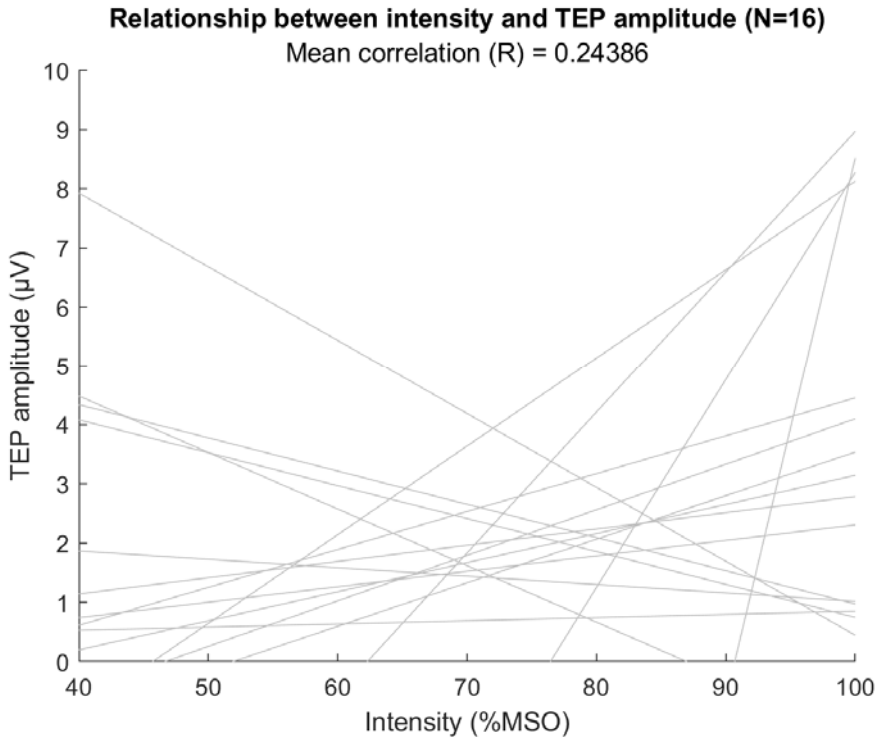

Supplementary Figure 5 - Relationship between stimulation intensity and early TEP amplitudes. Stimulation intensities were corrected across targets based on calculated maximal induced E-field.

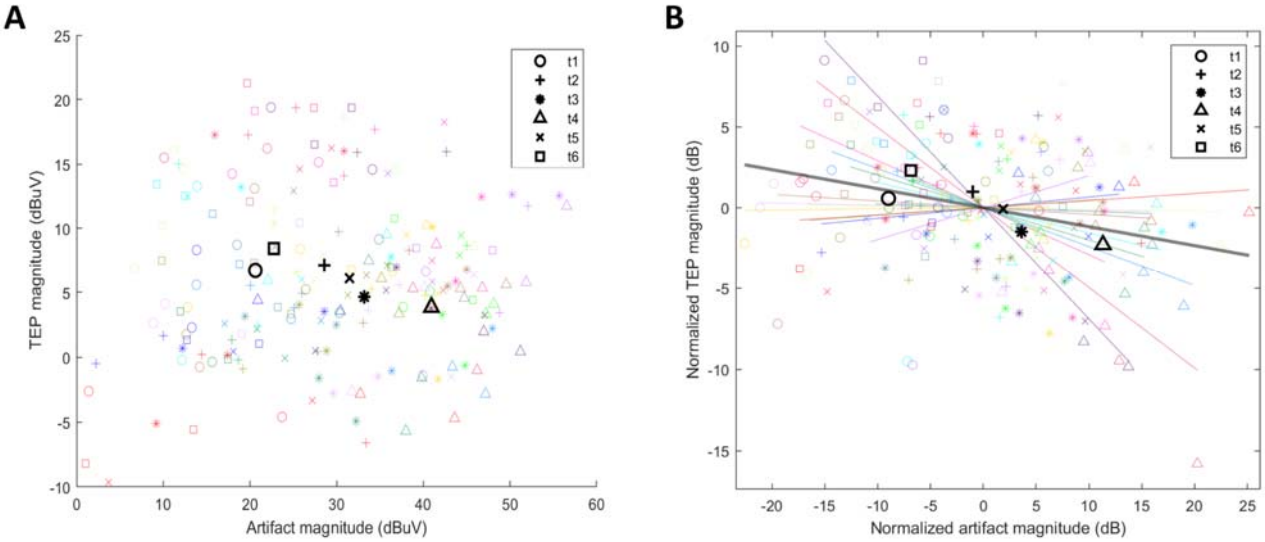

Supplementary Figure 6 - Relationship between early TEP amplitudes and artifact amplitudes. Shape of scatter points indicate target site, with one color per subject; black points represent the mean for each target across subjects. Normalized values in B were obtained by subtracting each subject's mean response magnitude (in dB). Colored lines in B represent linear fit of points across targets within each subject; bold gray line indicates linear fit of the mean values.

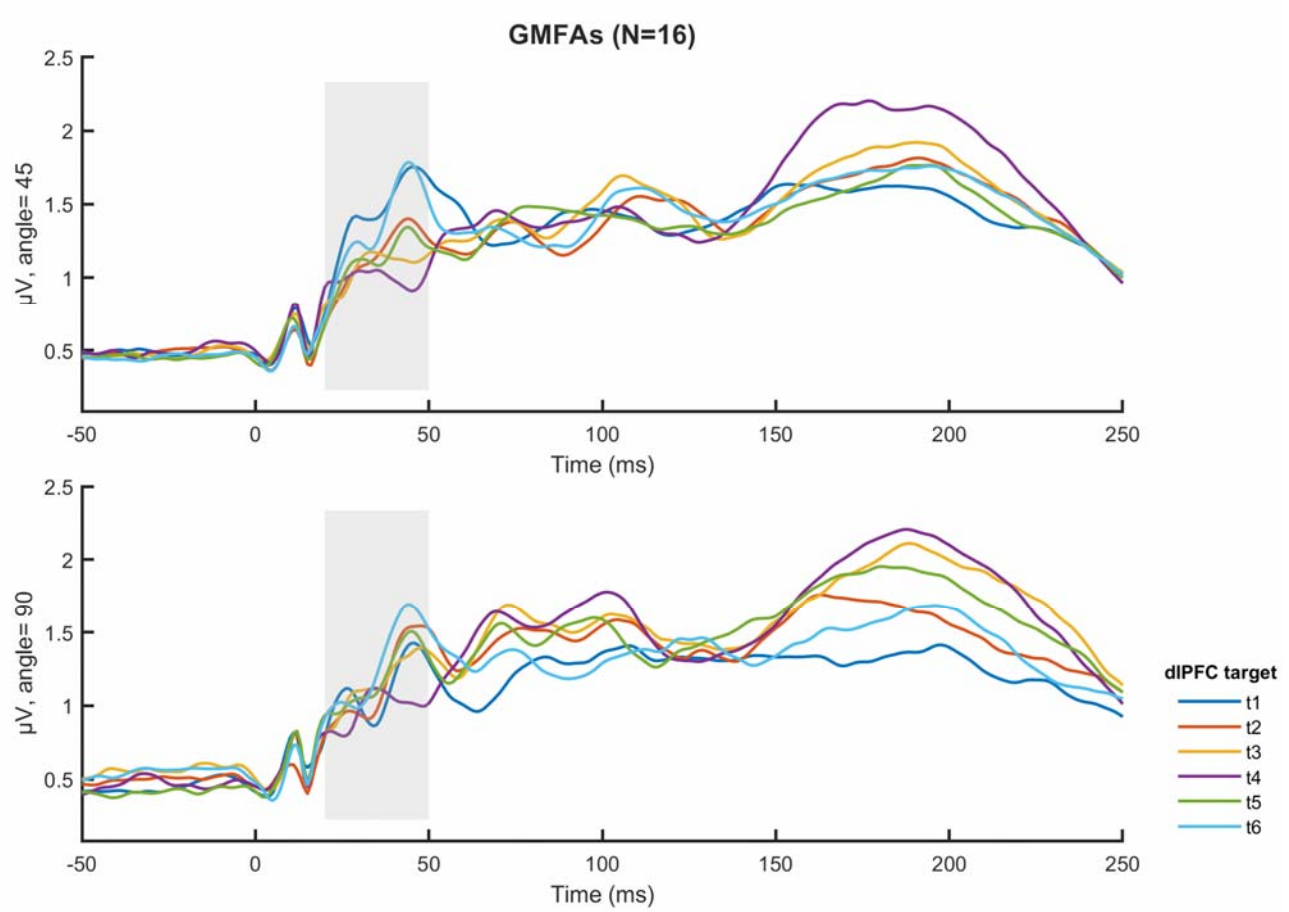

Supplementary Figure 7 - Mean GMFAs across targets (N=16). Upper panel represents 45 degrees coil angle and the lower panel represents 90 degrees coil angle.